Optical decoherence and spectral diffusion at 1.5 μm in $Er^{3+}:Y_2SiO_5$ versus magnetic field, temperature, and Er^{3+} concentration

Thomas Böttger*
Department of Physics, University of San Francisco, 2130 Fulton Street, San Francisco, California 94117, USA
and Department of Physics, Montana State University, Bozeman, Montana 59717, USA

C. W. Thiel,† Y. Sun,‡ and R. L. Cone§
Department of Physics, Montana State University, Bozeman, Montana 59717, USA
(Received 28 October 2005; published 1 February 2006)

The mechanisms and effects of spectral diffusion for optical transitions of paramagnetic ions have been explored using the inhomogeneously broadened 1536 nm $^4I_{15/2} \rightarrow {}^4I_{13/2}$ transition in $Er^{3+}:Y_2SiO_5$. Using photon echo spectroscopy, spectral diffusion was measured by observing the evolution of the effective coherence lifetimes over time scales from 1 μs to 20 ms for magnetic-field strengths from 0.3 to 6.0 T, temperatures from 1.6 to 6.5 K, and nominal Er^{3+} concentrations of 0.0015%, 0.005%, and 0.02%. To understand the effect of spectral diffusion on material decoherence for different environmental conditions and material compositions, data and models were compared to identify spectral diffusion mechanisms and microscopic spin dynamics. Observations were successfully modeled by $Er^{3+}-Er^{3+}$ magnetic dipole interactions and Er^{3+} electron spin flips driven by the one-phonon direct process. At temperatures of 4.2 K and higher, spectral diffusion due to ^{89}Y nuclear spin flips was also observed. The success in describing our extensive experimental results using simple models provides an important capability for exploring larger parameter spaces, accelerating the design and optimization of materials for spatial-spectral holography, and spectral hole-burning devices. The broad insight into spectral diffusion mechanisms and dynamics is applicable to other paramagnetic materials, such as those containing Yb^{3+} or Nd^{3+}.

DOI: 10.1103/PhysRevB.73.075101 PACS number(s): 42.70.−a, 76.30.−v, 42.50.Md, 32.70.Jz

I. INTRODUCTION

Spectral diffusion in the optical spectra of rare-earth ions is important from the perspectives of both basic science and emerging technologies, and the significance of the resulting decoherence is well known in the fields of spin resonance[1–6] and optical spectroscopy.[7–11] Spectral diffusion results from time-dependent perturbations of each ion's transition frequency due to the dynamic nature of the ion's environment. Over time, the accumulated frequency shifts cause each ion to perform a limited random walk in frequency or to "diffuse" through the optical spectrum. When this "spectral diffusion" is averaged over the ensemble of ions probed in the material, an individual homogeneous packet of ions with initial spectral width Γ_h appears to broaden over time to attain a frequency distribution determined by the spectral diffusion mechanism. This time-dependent broadening also leads to a progressive increase in the rate of phase decoherence.

In optical materials, decoherence and spectral diffusion can arise from a wide variety of sources, such as spin-spin interactions, dynamic structural rearrangement, and motion of charge defects. Spectral diffusion occurs when a significant frequency-shifting interaction is present together with a mechanism that modulates the magnitude of that interaction. For rare-earth-doped materials at low temperatures, an important mechanism for spectral diffusion is the magnetic dipole-dipole interaction between each optically active ion and the other electronic and nuclear spins in the host. This is particularly true for odd-electron ions due to their strong electronic paramagnetism. By studying spectral diffusion in these materials, fundamental insight and practical information are obtained concerning the optical properties of the active ions and the dynamic interactions within the host material.

In this paper, we present experimental and theoretical studies of decoherence and spectral diffusion in the material $Er^{3+}:Y_2SiO_5$. Detailed observations were carried out on the Er^{3+} $^4I_{15/2} \rightarrow {}^4I_{13/2}$ transition at 1536 nm using both photon echo and stimulated photon echo spectroscopy. Details of the echo decays and evolution of the effective homogeneous linewidth were modeled over a broad parameter space of magnetic-field strength, crystal temperature, and Er^{3+} dopant concentration. That analysis clearly demonstrated the importance of (i) magnetic dipole-dipole interactions between Er^{3+} ions and (ii) the one-phonon direct process driving Er^{3+} spin flips at low temperature. The measurements and models provide comprehensive insight into the spectral diffusion dynamics of Er^{3+} materials and, by direct analogy, a broader range of similar paramagnetic rare-earth-doped materials, such as those containing Yb^{3+} or Nd^{3+}.

In many spatial spectral holography (SSH) and spectral hole burning (SHB) applications, stimulated photon echoes are used to store and interrogate temporally structured optical data pulse patterns as spectral gratings in the ground- and excited-state populations of inhomogeneously broadened rare-earth-doped materials. Understanding, predicting, and controlling spectral diffusion is particularly important for these applications since a material's effective homogeneous

linewidth and coherence lifetime determine the achievable spectral resolution. The development and optimization of practical SSH and SHB materials is important for applications, including real-time multi-gigahertz signal processing, information storage in communication systems and computing,[12–19] laser frequency stabilization relevant both to fundamental spectroscopy and device applications,[20–23] and quantum information applications.[24–26] By employing Er^{3+} materials, such as $Er^{3+}:Y_2SiO_5$,[11,23] $Er^{3+}:LiNbO_3$,[11] $Er^{3+}:Y_2O_3$,[11] $Er^{3+}:KTP$,[11,21] and $Er^{3+}:YAG$,[11,27] these applications can benefit from the extensive technological infrastructure already developed for the telecommunication band at 1.5 μm, including high-quality fiber-optic components, diode lasers, phase and amplitude modulators, and erbium-doped fiber amplifiers. SSH and SHB device applications require fundamental material research, providing one of the central motivations for characterizing and understanding spectral diffusion to manage and control the impact on performance.[23,28]

The experimental characterization and theoretical understanding of the material physics gained from this study have allowed the properties of these materials to be optimized by choosing the specific operating conditions and material composition required by individual device applications. This approach also provides guidance for the development of materials that incorporate Er^{3+} or other paramagnetic ions.

After introduction of the basic material properties in Sec. II, a description of the stimulated photon echo measurements and how the observed echo decays can be modeled to extract information about the underlying microscopic spin dynamics is given in Sec. III. Sections IV–VI detail the dependence of spectral diffusion on magnetic field, crystal temperature, and Er^{3+} concentration.

II. $Er^{3+}:Y_2SiO_5$ MATERIALS BACKGROUND

The material Y_2SiO_5 is well known as an excellent host for achieving ultraslow optical decoherence by minimizing the magnetic moments in the host lattice and, consequently, reducing decoherence due to nuclear and electronic spin fluctuations.[29–31] The constituent ions in Y_2SiO_5 have small magnetic moments ($-0.137\ \mu_N$ for ^{89}Y) or small natural abundance of magnetic isotopes (4.7% with $-0.554\ \mu_N$ for ^{29}Si, 0.04% with $-1.89\ \mu_N$ for ^{17}O).

For $Er^{3+}:Y_2SiO_5$, spectral hole burning at 1536 nm occurs for the lowest energy Er^{3+} $^4I_{15/2} \rightarrow {}^4I_{13/2}$ transition by population storage in the long-lived $^4I_{13/2}$ excited state ($T_1 = 11.4$ ms).[32] The first two-pulse photon echoes in $Er^{3+}:Y_2SiO_5$ were reported in 1997, where coherence lifetimes as long as 0.6 ms were observed.[31] Those investigations also reported the presence of spectral diffusion. The long coherence lifetimes triggered a number of SSH and SHB proof-of-principle device demonstrations, including real-time address header decoding for optical data routing,[13] correlation of phase-shift-keyed pulse codes,[14] radio frequency spectrum analysis,[17] photon echo amplification,[33] and applications to laser frequency stabilization.[20–22] Recently, our Er^{3+} material optimization allowed the demonstration of higher bandwidth (0.5 GHz) analog signal processing at temperatures of 4.2 K,[16] and those demonstrations can be extended to bandwidths of >20 GHz with current material development.[34] The SSH and SHB technologies may enable all-optical memory, switching, and processing at communication wavelengths and exploit telecom hardware for more general applications.

The crystal Y_2SiO_5 (also called yttrium silicate, yttrium orthosilicate, YSO, or YOS) has eight formula units per monoclinic cell and belongs to the space group C_{2h}^6 (C2/c, number 15). The monoclinic cell of Y_2SiO_5 has dimensions $a = 10.410$ Å, $b = 6.721$ Å, $c = 12.490$ Å, and $\beta = 102.39°$, where β defines the angle between a and c, giving $V = 853.51$ Å^3 for the unit-cell volume.[35] The unit cell contains 16 Y^{3+} ions, and the total Y^{3+} density is 1.83×10^{22} cm^{-3}. The Y^{3+} ions equally occupy two crystallographically inequivalent sites of C_1 symmetry, each with two magnetically inequivalent orientations, and the Er^{3+} ions substitute for Y^{3+} host ions without charge compensation. The Er^{3+} ionic radius is very similar to that of Y^{3+}, and we believe the occupancy of the two Y^{3+} sites by Er^{3+} dopant ions is nominally equal, unlike the cases of $Pr^{3+}:Y_2SiO_5$ and $Eu^{3+}:Y_2SiO_5$.[36] The work reported here focused on the lowest energy transition between the Zeeman-split levels of site 1. At zero magnetic field, the vacuum wavelengths are 1536.48 nm (site 1) and 1538.90 nm (site 2) for the lowest energy $^4I_{15/2}$ to $^4I_{13/2}$ transitions of Er^{3+} at the two crystallographic sites.[32]

All crystals were grown by Scientific Materials Corp. (Bozeman, MT) using the Czochralski method and were transparent and colorless. There are three mutually perpendicular optical extinction axes in Y_2SiO_5: the crystal's $\boldsymbol{b}$ axis and the $\boldsymbol{D}_1$ and $\boldsymbol{D}_2$ axes that correspond to the optical extinction directions when the crystal is viewed along the $\boldsymbol{b}$ axis between crossed polarizers.[37] All crystals were oriented by Laue x-ray diffraction and polished to optical quality, and the crystal was precisely oriented on the sample holder using crossed polarizers. The $Er^{3+}:Y_2SiO_5$ crystals investigated had nominal Er^{3+}-dopant concentrations of 0.02% (growth number 2-430), 0.005% (growth number 6-429), and 0.0015% (growth number 1-544) atomic percent substitution for Y^{3+} and the relative Er^{3+} concentration of each crystal was verified for site 1 by measuring the integrated absorption coefficient with laser absorption at 5 K.

III. STIMULATED PHOTON ECHO MEASUREMENTS

Coherence measurements on inhomogeneously broadened transitions are a sensitive probe of spectral diffusion. They also overcome the resolution limits imposed by laser frequency jitter, power broadening, and time resolution typically found in other nonlinear techniques, such as direct spectral hole-burning measurements.[38] In this study, stimulated photon echo spectroscopy was used to measure the evolution of the homogeneous optical linewidth over a range of timescales from 1 μs to 20 ms.

A. Experimental details

The $Er^{3+}:Y_2SiO_5$ crystals were mounted in an Oxford Instruments Spectromag cryostat providing magnetic-field

strengths up to $B=8$ T. The crystals were aligned with the light propagating along the $\boldsymbol{b}$ axis, the polarization along the $\boldsymbol{D}_2$ axis, and the magnetic field along $\boldsymbol{D}_1$. An external cavity diode laser with output power of ~1.8 mW was amplified by an erbium-doped fiber amplifier to give 15 mW at the sample. A 165 MHz acousto-optic modulator gated the amplified laser beam to generate the pulses for echo excitation. For most experiments, the beam was focused inside the crystal to a waist of radius $w_0 \sim 25$ μm. Typical $\pi/2$-pulse widths were ~500 ns, corresponding to a 2 MHz spectral width that minimized the sensitivity of the measurements to laser frequency fluctuations. Photon echo signals were detected using a fast InGaAs photodiode and processed with a digital oscilloscope interfaced with a data-acquisition computer.

Stimulated echo decays were recorded as a function of pulse separation in the three-pulse excitation sequence. Both t_{12}, the delay between the first and second pulse in the three-pulse excitation sequence, and the "waiting time" T_W, the delay between the second and third pulse, were varied. For measurements described as t_{12} decays, T_W was held fixed, and for measurements described as T_W decays, t_{12} was held fixed. Typical t_{12} decays for 0.02 % $Er^{3+}:Y_2SiO_5$ in a magnetic field of 2.25 T and at 1.6 K are presented in Fig. 1(a) for values of T_W from 0 μs (equivalent to a two-pulse photon echo decay) to 1000 μs. Each echo decay curve was normalized to the echo intensity at the shortest delay measured for that curve. Stimulated photon echo decays for short waiting times were nonexponential, indicating the presence of spectral diffusion occurring on the time scale of the echo sequence. Longer waiting times yielded exponential decays with increasing decay rates that saturated at values determined by the temperature, concentration, magnetic-field orientation, and magnetic-field magnitude. Figure 1(b) shows typical stimulated photon echo T_W decays under the same experimental conditions for t_{12} values ranging from 1 to 15 μs. Individual decays are normalized to the echo intensity for a time delay of $T_W=0$ and displayed on double-logarithmic scales.

Each data point shown in Fig. 1 has been averaged over 16 samples, so that a single decay curve was the result of ~1000 intensity measurements. Stimulated echo t_{12} decays were measured for specific values of the waiting time T_W; typically, 30 different waiting times were chosen. Hence, ~30 000 individual intensity measurements were required for each unique parameter set of magnetic field, temperature, and Er^{3+} concentration. The scope of the experimental work presented in this paper entails the effort of measuring and analyzing well over 1000 echo decay curves generated from more than 1 000 000 individual intensity measurements.

A strong modulation was observed in the two-pulse echo decays for $B<0.3$ T and was attributed to superhyperfine coupling between Er^{3+} and neighboring ^{89}Y nuclear spins. At these low fields, the echo pulse sequence simultaneously excites transitions from multiple superhyperfine levels, producing a coherent interference that causes the echo modulation. The echo modulation was only observed at very low fields and did not influence the results or analysis presented here. We note that a detailed study of this effect could be used to characterize the superhyperfine coupling and local environment of the Er^{3+} impurity.

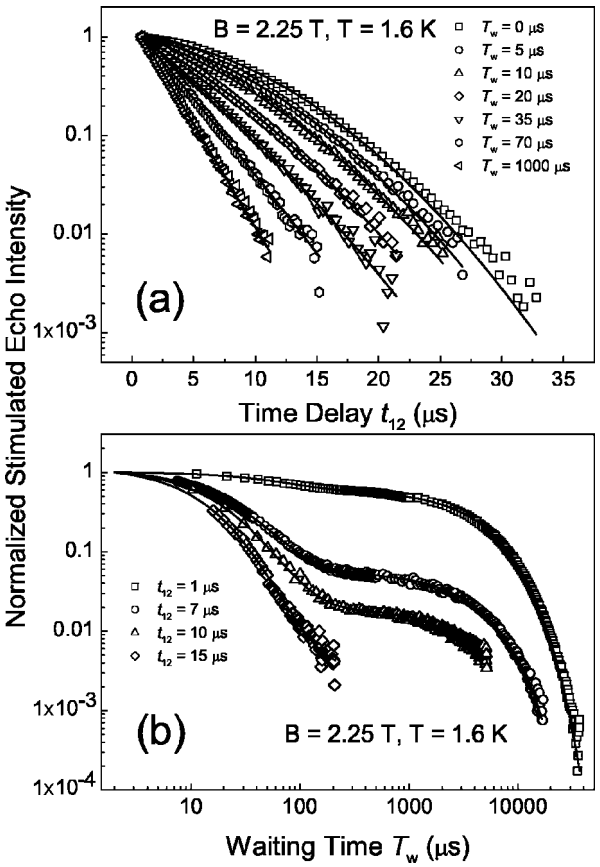

FIG. 1. Stimulated photon echo decays for 0.02% $Er^{3+}:Y_2SiO_5$ in a magnetic field of $B=2.25$ T at $T=1.6$ K (a) as the waiting time was varied between 0 and 1000 μs (t_{12} echo decays), and (b) as the pulse separation t_{12} was varied between 1 and 15 μs (T_W echo decays). Note that all echo decay curves were normalized to the intensity of the first data point. Solid lines are least-squares fits to Eq. (3) with Γ_{eff} given by Eq. (4).

B. Effect of spectral diffusion on stimulated echo decays

The stimulated photon echo is produced by a three-pulse excitation sequence and can be thought of as a modified two-pulse echo with a pulse delay of t_{12}, where the second π pulse is divided into two $\pi/2$ pulses separated by the waiting time T_W.[39] The first pulse prepares the system by placing each ion in a coherent superposition of the ground and excited state. During the delay t_{12} between pulse 1 and 2, the phase of the superposition state evolves according to the ion's instantaneous transition frequency. The second pulse stores each ion's total accumulated phase as a population difference between the ground and excited states. Thus, a frequency-dependent population grating is produced between the ground and excited states with a period given by $1/t_{12}$. This grating decays with the lifetime of the excited state T_1 due to population relaxation to the ground state. When a short $\pi/2$ pulse is applied after a waiting time T_W, the coherence stored in the population grating is rephased after an additional time delay of t_{12} and a stimulated photon echo is emitted.

In the absence of spectral diffusion, the intensity of the emitted stimulated photon echo is determined by the

product of two factors. The first factor is proportional to $\exp(-2T_W/T_1)$ and describes the population decay during T_W. The second factor is proportional to $\exp(-4t_{12}/T_2)$ and describes the effect of decoherence during the t_{12} sections of the echo sequence due to the homogeneous linewidth with full width at half maximum of $\Gamma_h = 1/(\pi T_2)$. These two factors give the well-known exponential form of the stimulated photon echo intensity (see, for example, Ref. 39)

$$I(t_{12}, T_W) = I_0 \exp\left\{-\frac{2T_W}{T_1}\right\}\exp\{-4t_{12}\pi\Gamma_h\}, \quad (1)$$

where I_0 is the maximum echo intensity.

When spectral diffusion is present, the behavior of the echo intensity can deviate from the simple exponential expression given by Eq. (1). For a fixed value of T_W, the nonexponential echo decay curves that result from spectral diffusion often can be described approximately by the empirical form first proposed by Mims[3]

$$I(t_{12}) = I_0 \exp\left\{-2\left(\frac{2t_{12}}{T_M}\right)^x\right\}, \quad (2)$$

where the exponent x determines the shape of the decay curve and the effective phase memory lifetime T_M is the time over which the material coherence decays to $1/e$ of its initial electric field amplitude, or $1/e^2$ of its initial intensity. Spectral diffusion during the T_W section of the echo sequence will generally cause both T_M and x to vary for different values of T_W. Although there is usually no simple relationship between T_M and precise spectral hole width or shape, the empirical form of Eq. (2) and T_M are nonetheless extremely valuable for describing and characterizing material decoherence in the presence of spectral diffusion.

To gain a fundamental understanding of the spectral diffusion process and its effect on material coherence, we must consider specific physical models for the mechanisms and dynamics responsible for perturbing the transition frequencies. Paramagnetic ions, such as Er^{3+} (and other ions with degenerate electronic states), are particularly sensitive to fluctuations in the local magnetic fields due to the large magnetic moments of their electronic states. Magnetic dipole-dipole interactions are thus a leading source of spectral diffusion in these materials. Through magnetic dipole-dipole interactions, the transition energies of each paramagnetic ion depends on the orientations of all other magnetic moments in the host material; therefore, whenever an electronic or nuclear spin changes its orientation, all the paramagnetic ions in its environment are perturbed, resulting in spectral diffusion.

The effects of magnetic dipole-dipole interactions on resonance linewidths and spin transients in nuclear magnetic resonance (NMR) and electron paramagnetic resonance (EPR) have been investigated extensively both experimentally and theoretically over the past six decades.[4,40,41] Spectral diffusion due to magnetic dipole-dipole interactions in a typical solid can exhibit a complex behavior that is difficult to describe over a wide range of conditions because of the large number of spins, the long range of the interaction, and the dynamic nature of the generally anisotropic spin-spin and spin-lattice interactions. From the earliest treatments of the dipolar broadening observed in EPR and NMR signals,[40,42,43] the theory has been progressively extended to consider different statistical models for the diffusion process, first under limiting conditions,[1–3] which eventually led to more general treatments.[5,6,44] In much the same way that the theory of spin transients provided the basis for the theory of optical transients, the theoretical framework developed to describe the effects of spectral diffusion in NMR and EPR measurements can be applied to optical coherent transient and spectral hole-burning experiments.

Following the traditional approach used in EPR, the additional decoherence caused by spectral diffusion during the t_{12} and T_W sections of the echo sequence may be approximately treated by introducing two factors into Eq. (1).[45] The first of these factors describes the spectral diffusion that occurs during the two t_{12} delays and, therefore, only depends on t_{12}. The evolution of the linewidth during the t_{12} sections of the echo sequence results in a progressive loss of phase coherence between ions, causing the echo decays to become nonexponential. The effect of this process on the echo intensity has been described by Klauder and Anderson[2] for the high-temperature limit by modeling the fluctuations in the local magnetic field experienced by each ion as a Lorentzian diffusion process (the sudden-jump model). Spectral diffusion also introduces a second decay factor into the echo intensity that arises from linewidth broadening during T_W; this broadening affects the observed decay rate of the echo due to the additional decoherence during the last t_{12} section of the echo sequence. Using the Lorentzian diffusion model, the form of this decay factor has been discussed by Mims for the high-temperature limit.[3] The forms of these two contributions may also be derived from more rigorous treatments of the sudden-jump model.[5] To extend these results to low temperatures, we compared the high-temperature limits to temperature-dependent calculations. For example, the integral representations of the echo decay function derived by Hu and Walker[6] for the sudden-jump model may be expanded to lowest order and compared to the high-temperature limits to obtain the general forms of the simple decay factors.

The stimulated echo decay function given by Eq. (1) was generalized to incorporate these spectral diffusion effects by replacing the constant homogeneous linewidth with a time-dependent "effective" linewidth $\Gamma_{eff}(t_{12}, T_W)$

$$I(t_{12}, T_W) = I_0 \exp\left\{-\frac{2T_W}{T_1}\right\}\exp\{-4t_{12}\pi\Gamma_{eff}(t_{12}, T_W)\}. \quad (3)$$

The functional form of $\Gamma_{eff}(t_{12}, T_W)$ derived from the spectral diffusion decay factors is given by

$$\Gamma_{eff}(t_{12}, T_W) = \Gamma_0 + \frac{1}{2}\Gamma_{SD}[Rt_{12} + \{1 - \exp(-RT_W)\}], \quad (4)$$

where Γ_0 is the linewidth in the absence of spectral diffusion (including effects such as the single-ion homogeneous line-

width and instantaneous spectral diffusion), Γ_{SD} is the full width at half maximum of the dynamic distribution of transition frequencies due to dipole-dipole interactions, and R is the characteristic rate of the spectral diffusion process given by the sum of the upward and downward spin-flip transition rates of the perturbing spins.

The form of Eq. (4) was chosen to emphasize the deviations from Eq. (1) caused by spectral diffusion. For example, if either the spectral diffusion is very small ($\Gamma_{SD} \ll \Gamma_0$) or the measurement is performed on a time scale much shorter than the inverse spin-flip rate ($t_{12}, T_W \ll 1/R$), the echo decay function given by Eq. (3) reduces to the simple form of Eq. (1). If more than one source of spectral diffusion is present, Eq. (4) may be modified by including additional terms in the effective linewidth that describe each source. This follows from the assumptions of a Lorentzian diffusion process and Lorentzian line shapes that were used to obtain Eq. (4). At much longer time scales, however, the linewidths may combine in a more complicated manner. In systems where broad distributions of rates are present, such as glasses, a more general treatment of the echo decay function may be required.[44]

The effective linewidth given by Eq. (4) is valid only in the limit $Rt_{12} \ll 1$ since it ignores correlations in the local field fluctuations caused by multiple spin flips. As the perturbing spins in the environment begin to undergo multiple spin flips, the decoherence due to subsequent spin flips partially cancels, resulting in a reduced echo decay rate.[1] In the limit $Rt_{12} \gg 1$, we expect the effective linewidth to become independent of T_W, approaching the approximate form[3,5]

$$\Gamma_{\mathrm{eff}}(t_{12}, T_W) \simeq \Gamma_0 + \Gamma_{SD}\sqrt{\frac{2}{\pi R t_{12}}}. \tag{5}$$

From Eq. (5) we can clearly see that the spectral diffusion contribution to the linewidth at long times decreases for very large t_{12} or R. This averaging effect is equivalent to the "motional narrowing" effects well-known, since the earliest magnetic resonance studies.[40,46]

The spectral diffusion dynamics may be most directly probed by examining the effective linewidth as $t_{12} \to 0$ so that Eq. (4) simplifies to

$$\Gamma_{\mathrm{eff}}(T_W) = \Gamma_0 + \frac{1}{2}\Gamma_{SD}[1 - \exp\{-RT_W\}]. \tag{6}$$

This expression represents the effective initial linewidth for very short t_{12} and approximately describes the behavior of the effective linewidth for cases where it is dominated by spectral diffusion during the waiting time, as is the case for large T_W. In this limit, the linewidth and rate that characterize the spectral diffusion process may be easily extracted from the data by measuring the effective linewidth as a function of T_W. In the limit of $RT_W \gg 1$, Eq. (3) and Eq. (4) predict simple exponential decays with a maximum effective linewidth given by $\Gamma_0 + \frac{1}{2}\Gamma_{SD}$, where the factor of $\frac{1}{2}$ enters because spectral diffusion during the waiting time only produces decoherence for the last t_{12} section of the echo sequence. In the frequency domain, this is equivalent to a single homogenous frequency bin of intrinsic width Γ_0 broadening into a Lorentzian with a full width at half maximum of $\Gamma_0 + \Gamma_{SD}$ due to spectral diffusion over T_W. We note that in the corresponding time-resolved hole-burning measurement, where a spectral hole is probed by scanning a narrowband laser across the absorption, an additional broadening of Γ_0 will be observed due to the convolution of the single-atom readout response with the population frequency distribution, giving a minimum observed hole width of $2\Gamma_0 + \Gamma_{SD}$.

When significant spectral diffusion is present, there is generally a complicated relationship between the linewidth and the empirical phase memory lifetime T_M defined by Eq. (2). Using the spectral diffusion model described by Eqs. (3) and (4), T_M can be calculated from the material parameters Γ_0, Γ_{SD}, and R to be

$$T_M = \frac{1}{b}\left(-a + \sqrt{a^2 + \frac{2b}{\pi}}\right)$$

$$a = \Gamma_0 + \frac{1}{2}\Gamma_{SD}[1 - \exp(-RT_W)]$$

$$b = \frac{1}{2}\Gamma_{SD}R. \tag{7}$$

Examining Eq. (7), we see that the relationship $T_M = 1/(\pi\Gamma_{\mathrm{eff}})$ only holds for the limits $\Gamma_{SD} \to 0$ or $R \to 0$; nevertheless, the effective phase memory time T_M remains valuable as a simple method for characterizing the decoherence time scale.

Combining the echo intensity given by Eq. (3) with the different forms of the effective linewidth, measured stimulated echo intensities can be accurately described over a wide range of t_{12} and T_W time scales using the physical parameters Γ_0, Γ_{SD}, and R. Furthermore, analyzing the behavior of R and Γ_{SD} values extracted from the data provides direct insight into the mechanisms responsible for spectral diffusion.

C. Variation of echo intensity with t_{12}

Using the decay function given by Eqs. (3) and (4), the complete family of nonexponential t_{12} decay curves for different waiting times T_W may be described with just three parameters Γ_0, Γ_{SD}, and R. As an illustration of this, the open symbols in Fig. 1(a) represent measured echo intensities and the solid lines are fits of Eq. (3), with Γ_{eff} given by Eq. (4), showing excellent agreement. Both the shape of the echo decay curves and the variation in the echo decays for different values of T_W are well understood and accurately predicted by the theoretical spectral diffusion model. The small deviations of the fit from the data at large t_{12} for the first two curves with $T_W = 0$ and 10 μs are expected since those values of t_{12} begin to approach $1/R$. As previously discussed, this tendency for the data to decay more slowly at large t_{12} indicates a transition to the "motional-narrowing" regime described by Eq. (5).

To robustly extract the underlying information regarding the spectral diffusion process, each echo decay curve was fit to Eqs. (3) and (4) to determine the effective linewidth Γ_{eff} at

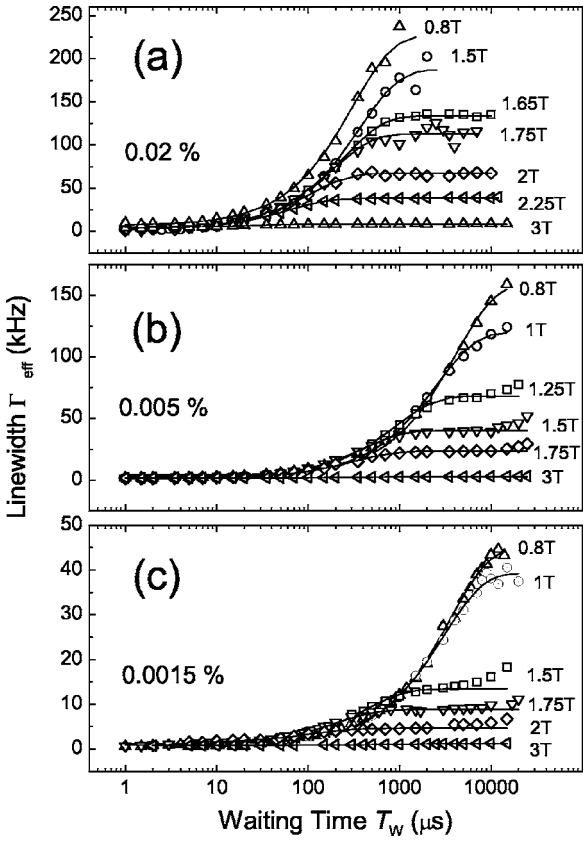

FIG. 2. Evolution of the effective linewidth for site 1 in (a) 0.02%, (b) 0.005%, and (c) 0.0015% $Er^{3+}:Y_2SiO_5$ at 1.6 K as the waiting time T_W was varied. The magnetic field was varied over the range from $B=0.8$ T to $B=3$ T. Solid lines are least-squares fits to the data using Eq. (6).

$t_{12}=0$. This approach isolates the simple dependence of the echo intensity on T_W and minimizes biases in the spectral diffusion parameters due to motional narrowing effects that occur at large values of t_{12}. This method also provides a clear picture of the time evolution of the linewidth that is described by Eq. (6). Values of the effective linewidth for different waiting times T_W are presented in Figs. 2 and 3 for a range of experimental conditions, where each data point was extracted from fitting a full experimental stimulated echo decay curve. Spectral diffusion was clearly observed in the significant broadening of the linewidth as T_W was increased. The linewidth rapidly broadened until a plateau was reached where the spectral diffusion contribution to the linewidth attained its maximum value. These experimentally observed variations in the effective linewidth were analyzed to determine the magnitude Γ_{SD} and rate R of the spectral diffusion process that characterizes the interaction dynamics.

D. Variation of echo intensity with T_W

The echo decay function given by Eqs. (3) and (4) was used to fit the T_W decay curves like those shown in Fig. 1(b). Solid lines are fits to the experimental decays, again showing excellent agreement with the spectral diffusion model. Rapid initial decays are due to spectral diffusion "smearing out" the

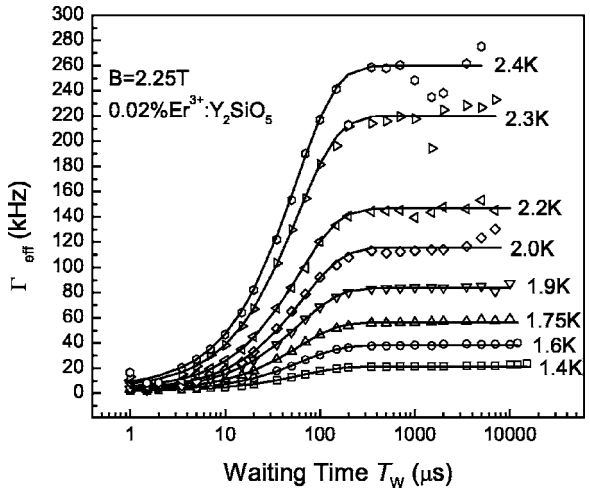

FIG. 3. Evolution of the effective linewidth for site 1 in 0.02% $Er^{3+}:Y_2SiO_5$ at $B=2.25$ T as the waiting time T_W was varied. The temperature was varied over the range from $T=1.4$ K to $T=2.4$ K. Solid lines are least-squares fits to the data using Eq. (6).

coherence stored in the population grating during T_W. This decay process is enhanced for larger t_{12} values since the frequency shifts during T_W produce phase errors during the last section of the echo sequence that are directly proportional to t_{12}. At longer times, the echo intensity decays exponentially with $T_1/2$ due to population relaxation from the excited state, as indicated by Eq. (3). The same parameters were independently obtained by separately fitting both the t_{12} and T_W decays, confirming the ability of the spectral diffusion model to describe both types of stimulated echo decay curves.

It is important to note that the T_W echo decays did not exhibit any components with time constants longer than T_1. This indicates that population storage in the excited state was the only significant hole-burning mechanism observed and that population storage in the upper Zeeman sublevel of the ground-state Kramers doublet was not an effective SHB mechanism under these experimental conditions. Electronic sublevel storage has been observed in $Er^{3+}:Y_2SiO_5$ using time-resolved spectral hole burning[47] and can provide longer hole lifetimes when the Er^{3+} spin-lattice relaxation rate is slower than the excited-state relaxation rate.[48,49]

IV. DEPENDENCE OF SPECTRAL DIFFUSION ON MAGNETIC FIELD

The magnetic-field dependence of the observed linewidths was used to identify the dominant spectral diffusion mechanism and to show that magnetic-field strength together with Er^{3+} dopant concentration may be chosen to design materials that provide specific linewidths under operating conditions required for given applications. For example, with a magnetic field of $B=2$ T, quite significant spectral diffusion was observed for 0.02% $Er^{3+}:Y_2SiO_5$, whereas it was almost negligible for 0.0015% $Er^{3+}:Y_2SiO_5$ at that same field. Representative stimulated echo decay measurements at 1.6 K, shown in Fig. 2 as a function of T_W for magnetic fields from 0.8 T up to 3 T, demonstrate that larger magnetic fields dra-

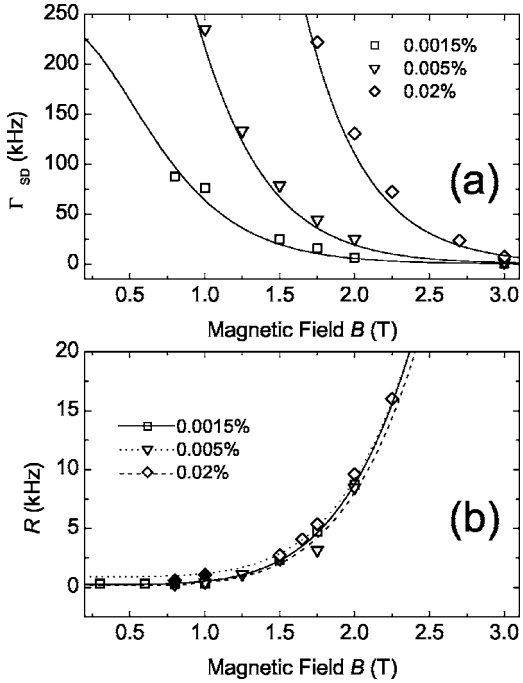

FIG. 4. (a) Measured spectral diffusion linewidth Γ_{SD} and (b) relaxation rate R as a function of magnetic field for 0.0015%, 0.005%, and 0.02% $Er^{3+}:Y_2SiO_5$ at 1.6 K; solid symbols in (b) were estimated using the method discussed in Sec. IV B. The lines are least-squares fits using Eqs. (9) and (11), respectively, with the parameters summarized in Table I.

matically suppress spectral diffusion. Together, these observations indicate that the spectral diffusion is not caused by nuclear spin flips, which would be relatively insensitive to the magnitude of the field,[9] but is caused primarily by $Er^{3+}-Er^{3+}$ interactions. Evidence for ^{89}Y nuclear spin flips contributing to spectral diffusion was also found at higher temperatures, as discussed in Sec. V B.

Using the spectral diffusion model, the time evolution of the effective linewidth observed in Fig. 2 was described by Eq. (6) and the fits shown in Fig. 2 as solid lines are in excellent agreement with the measurements. The spectral diffusion parameters Γ_{SD} and R obtained from these fits are plotted in Fig. 4 as a function of the external magnetic-field strength for each sample studied. Both Γ_{SD} and R clearly show strong magnetic-field dependence, with Γ_{SD} decreasing and R increasing for larger magnetic fields.

A. Maximum linewidths and identification of sources of spectral diffusion

To understand and interpret the observed magnetic-field dependence of the spectral diffusion linewidth Γ_{SD}, we examined the nature and strength of the interactions of Er^{3+} ions with the magnetic dipoles in their environment. A local perturbing field B_{loc} due to the ion's environment shifts the optical transition between the Er^{3+} ground and excited states with g factors of g_g and g_e, by $\Delta\nu=\frac{1}{2}(g_g-g_e)h\mu_B B_{loc}$, where μ_B is the Bohr magneton (with an optical shift factor of $\frac{1}{2}(g_g-g_e)=0.55$ for site 1 and $\boldsymbol{B}\|\boldsymbol{D}_1$).[32]

Consequently, the distribution of Er^{3+} transition frequencies is directly related to the total distribution of B_{loc} values at each ion resulting from the combined effect of all the magnetic moments in its environment. If the perturbing magnetic moments are described by a g factor of g_{env} and are randomly distributed throughout the crystal lattice with a density of n_{env}, the average broadening will be[4,40,50]

$$\Gamma_{max}=\frac{\pi}{9\sqrt{3}}\frac{\mu_0|g_g-g_e|g_{env}\mu_B^2 n_{env}}{h}, \tag{8}$$

where Γ_{max} is the full width at half maximum frequency broadening due to the magnetic dipole-dipole interactions under the assumption of isotropic g tensors, μ_0 is the permeability of vacuum, and h is Planck's constant.

The dipolar broadening described by Γ_{max} results from the random distribution of dipoles in the lattice and is generally composed of both static and dynamic contributions. The dynamic component directly corresponds to the observed spectral diffusion broadening, while the static component of Γ_{max} does not contribute to the time evolution of the echo intensities. As the temperature decreases, or the magnetic field increases, the perturbing moments tend to align preferentially with the external magnetic field, reducing the dynamic component of the dipolar linewidth and, therefore, reducing the magnitude of the spectral diffusion.

The temperature dependence of the dynamic linewidth may be obtained from any of several approaches, such as the method of moments,[42,43,51,52] statistical arguments,[44] or the general solutions for the sudden-jump model.[6] Following the approach used to establish the form of Eq. (4), we expanded the integral representations of the echo decay function given by Hu and Walker[6] and used Boltzmann statistics of the spin population to obtain the appropriate numerical factors and functional dependence. The temperature and field dependence of the spectral diffusion linewidth $\Gamma_{SD}(B,T)$ has the form

$$\Gamma_{SD}(B,T)=\Gamma_{max}\,\mathrm{sech}^2\left(\frac{g_{env}\mu_B B}{2kT}\right), \tag{9}$$

where k is the Boltzmann constant, Γ_{max} is given by Eq. (8), and all other quantities have the same meaning as in Eq. (8). As expected, spectral diffusion is dramatically suppressed for larger magnetic fields and lower temperatures due to the increase in magnetic order; in fact, the decrease in Γ_{SD} is directly proportional to the decrease in entropy of the system of perturbing moments.

From Eq. (9), the magnetic-field dependence of the spectral diffusion linewidth is entirely determined by the g factor of the perturbing moment if the temperature is held fixed. Consequently, the g factor of the perturbing moment can be determined by fitting Eq. (9) to the observed magnetic-field dependence; the extracted g factor may then be used to identify the source of spectral diffusion by comparing to known g factors for the various lattice constituents. Conversely, Eqs. (8) and (9) may be used to calculate the magnitude of the spectral diffusion broadening when the g factors of all the lattice constituents are known.

TABLE I. Material parameters describing optical decoherence and spectral diffusion for the $^4I_{15/2}$ to $^4I_{13/2}$ transition of Er^{3+} ions at site 1 in Y_2SiO_5 for $B \| D_1$.

Er^{3+} (%)	T (K)	Γ_{max} (kHz)	α_D (kHz/T^5)	R_0 (kHz)	Γ_0 (kHz)
0.02	1.6	4680	1.14×10^{-3}	0.9	3.2
0.005	1.6	820	1.09×10^{-3}	0.14	1.3
0.005	4.2	920			22
0.0015	1.6	240	1.16×10^{-3}	0.22	0.8

Fitting the measured Γ_{SD} dependence shown in Fig. 4(a) to Eq. (9) gave g values within 20% of the measured value $g_g=6.1$ for Er^{3+} at site 1 with $\boldsymbol{B}\|\boldsymbol{D}_1$,[32] clearly identifying flips of site 1 Er^{3+} ions as the source of spectral diffusion. Because the Er^{3+} ions residing at site 2 in the crystal have a much larger effective g factor of $g_g=14.7$ for this field orientation, Eq. (9) predicts that their contribution to the spectral diffusion is reduced to negligible values for all magnetic fields used in this work due to their nearly uniform alignment with the external field. For example, the site-2 contribution to the spectral diffusion of site 1 Er^{3+} ions is expected to be several orders of magnitude smaller than the site-1 contribution at 1 T, and we only expect the site-2 contribution to be significant for fields less than $\sim$0.5 T. Because the linewidths are much larger at low fields, echo decays could not be measured over a sufficient timescale for the site-2 contribution to become observable.

The magnetic moment of the ^{89}Y nuclear spins is small enough that their contribution to the spectral diffusion would be essentially independent of the magnetic field strength.[9] No contribution to the spectral diffusion from ^{89}Y was observed over the time scales investigated here due to the very slow flip rate of the nuclear spins; however, our evidence for an ^{89}Y contribution at higher temperatures is presented in Sec. V B.

Since the data indicate that Er^{3+} ions residing at site 1 are responsible for the observed spectral diffusion, the exact ground-state value of $g_{env}=6.1$ for $\boldsymbol{B}\|\boldsymbol{D}_1$ determined from our optical Zeeman spectroscopy[32] was used, leaving Γ_{max} as the only unknown parameter in Eq. (9). Least-squares fits to the Γ_{SD} experimental values using the fixed value of $g_{env}=6.1$ are plotted as the three lines in Fig. 4(a), showing excellent agreement with the data. The values of Γ_{max} obtained from the fits are presented in Table I.

If we use Eq. (8) to calculate the value of Γ_{max} from the measured g factors and the known density of environmental perturbers, which are Er^{3+} ions at site 1, we obtain values for each crystal that are a factor of ten smaller than the experimental values. This discrepancy mostly arises from the assumption of isotropic g factors used in the derivation of Eq. (8). When the g factors become significantly anisotropic, the induced magnetic moments are no longer parallel to the external magnetic field and the simple form of Eq. (8) must be modified to take into account the full tensor nature of the dipole-dipole interaction.[41,53] In fact, Eq. (8) may be used without correction only if either g_{env} is isotropic or if g_g and g_e are both isotropic. We may also use Eq. (8) without modification if the external field is applied along a direction that is parallel to a principle axis of all three g tensors. For $Er^{3+}:Y_2SiO_5$, the Er^{3+} ground- and excited-state g tensors are highly anisotropic and the principal axes for each state are not parallel; thus, the situation is quite complex. A complete treatment of the anisotropic dipole-dipole interaction strength is beyond the scope of this paper, but a very rough estimate may be obtained by using the results of Maryasov *et al.*[53] for axial symmetry and only considering the anisotropy in the $\boldsymbol{D}_1-\boldsymbol{D}_2$ plane.[32] When $\boldsymbol{B}$ is along the $\boldsymbol{D}_1$ direction, these estimates indicate that the site-1–site-1 dipole-dipole interaction is significantly enhanced by the magnetic anisotropy, as we observe, while the site-1–site-2 interaction is suppressed.

We also note that small uncertainties in the magnetic-field orientation, field strength, and internal sample temperature can have significant effects on the measured spectral diffusion linewidth. For example, a $\pm5^\circ$ misalignment of the magnetic field would cause Γ_{max} to vary by up to a factor of $\sim$2, and an uncertainty of only $\pm$0.1 K in the temperature causes the linewidths to change by up to 40%.

B. Spectral diffusion rate and identification of spin-flip mechanisms

Although the maximum broadening Γ_{SD} is determined by the nature of the dipolar interaction, the dynamics characterized by the rate R are determined by the spin-flip mechanisms that modulate the interaction. If all the spins in the environment were to maintain the same orientation over the time scale of the experiment (i.e., if $1/R \gg t_{12}, T_W$), the distribution of local magnetic fields in the crystal would be static and would not affect the photon echo decays. When the time scale of the spin fluctuations approaches the measurement time scale, the resulting modulation of the local fields causes each ion's transition energy to shift randomly, or "diffuse," during the measurement. Understanding the spectral diffusion requires an understanding of the microscopic spin-flip mechanisms; conversely, by characterizing the spectral diffusion process through the spin flip rate R, we gain fundamental insight into mechanisms driving the spin dynamics.

Figure 4(b) depicts experimental values of the spectral diffusion rate as a function of magnetic field for the 0.0015%, 0.005%, and 0.02% samples. For lower fields and higher concentrations where the maximum spectral diffusion broadening was not reached, estimates for R were obtained using the experimental values of Γ_{max} and Eq. (9) to estimate Γ_{SD}, allowing R to be determined from fitting the data to Eq. (6) with Γ_{SD} held fixed at its extrapolated value. Values of R estimated using this approach are indicated by solid symbols in Fig. 4(b). For cases where the spectral diffusion was com-

pletely suppressed at high fields, no R values can be extracted.

The magnitude of the experimental spectral diffusion rates in Fig. 4(b) explained why long-lived Zeeman sublevel storage was absent in the echo decays discussed in Sec. III D. Storage of population in the upper Zeeman level of the ground-state Kramers doublet can introduce a contribution to the stimulated echo that decays as the lifetime of the upper spin state, which can be significantly longer than the optical transition lifetime T_1 for some materials and experimental conditions.[48,49] Because the spectral diffusion rate R represents the sum of upward and downward spin-flip transition rates for the perturbing magnetic moments, site 1 Er^{3+} ions in this case, the spectral diffusion rates correspond directly to the decay rate for population storage in the ground-state Zeeman levels of site 1 Er^{3+} ions. From Fig. 4(b), the relaxation rates are kilohertz or greater, indicating that the Zeeman sublevel storage lifetime is actually significantly shorter than the 11.4 ms excited-state lifetime in $Er^{3+}:Y_2SiO_5$. The longest sublevel lifetimes are expected to occur for lower magnetic fields, but rapid decoherence and increased spectral diffusion at low fields restrict echo measurements to time scales too short to observe any Zeeman storage. Nevertheless, time-resolved hole-burning experiments that access longer time scales have revealed the presence of Zeeman-sublevel storage.[47]

To interpret the rate R, we note that spin flips of the perturbing dipole moments responsible for spectral diffusion may be induced through two mechanisms. The first is spin-lattice relaxation caused by interactions with phonon modes of the host lattice. The magnetic-field and temperature dependences of the spin-lattice relaxation rate are well understood and exhibit different types of behavior, depending on the nature of the dominant electron-phonon interaction mechanism;[41,54] furthermore, the spin-lattice relaxation rate may be strongly dependent on the magnetic-field orientation due to the anisotropy of the phonon coupling coefficients and the g factors.

The second mechanism responsible for driving spin flips is spin-spin relaxation in which the transverse components of the dipole-dipole interaction induce mutual spin "flip-flops" that cause pairs of antiparallel spins to flip simultaneously. Although this mechanism involves correlated spin flips and does not affect the net magnetization of the sample, the flip-flops can randomize local spin orientations and therefore contribute to spectral diffusion. Since a flip-flop process requires resonant antiparallel spins, inhomogeneous broadening of the spin-resonance frequency and the alignment of spins induced by an applied magnetic field can dramatically reduce electronic spin flip-flop rates. The flip-flop rate also depends on magnetic-field orientation due to anisotropy of the g factors. Since the Er^{3+} ions are randomly distributed throughout the lattice, there will not be a single rate, but a distribution of flip-flop rates determined by the distribution of ion environments.[55]

The spin-lattice relaxation and spin flip-flop processes contribute four terms to the total spin-flip rate for odd-electron ions given by

$$R(B,T) = \alpha_D g_{env}^3 B^5 \coth\left(\frac{g_{env}\mu_B B}{2kT}\right) + \alpha_R T^9 + \alpha_O \left\{\exp\left(\frac{\Delta}{kT}\right) - 1\right\}^{-1} + \alpha_{ff}\frac{g_{env}^4 n_{env}^2}{\Gamma_S}\,\mathrm{sech}^2\left(\frac{g_{env}\mu_B B}{2kT}\right). \quad (10)$$

The first term represents the one-phonon direct process for spin-lattice relaxation involving absorption or emission of a single phonon resonant with the perturbing moment's spin-flip transition, where α_D is a generally anisotropic constant characterizing the strength of the phonon coupling. The second term is the low-temperature form of the two-phonon Raman process in which the inelastic scattering of a high-energy phonon induces a transition between the spin states, where α_R is a coefficient describing the strength of this spin-lattice relaxation process. The third term describes the two-phonon resonant Orbach process where the perturbing spin's state is changed through excitation to a low-lying crystal-field level by phonon absorption and relaxation to a different spin state through phonon emission, where Δ is the energy of the crystal-field level and α_O is the coefficient describing the strength of this process. The last term represents the average flip-flop rate for spins with an inhomogeneously broadened paramagnetic resonance absorption linewidth of full width Γ_S, where α_{ff} is a constant that depends on the details of the crystal structure and resonance line shape. The temperature and field dependence of the flip-flop process arises from the probability for each spin pair in the lattice to be antiparallel and causes the flip-flop rate to decrease rapidly with increasing field or decreasing temperature due to the reduced number of antiparallel spin pairs.

The different magnetic-field and temperature dependences of each contribution to R allowed us to identify the physical process driving the spectral diffusion dynamics. As the magnetic field is increased, the direct-process rate rapidly increases, the flip-flop rate rapidly decreases, and the Raman and Orbach rates remain constant. Fitting Eq. (10) to the spectral diffusion rates R presented in Fig. 4(b) shows that they are best described by the form

$$R(B) = R_0 + \alpha_D g_{env}^3 B^5 \coth\left(\frac{g_{env}\mu_B B}{2kT}\right), \quad (11)$$

with the direct process as the dominant spin-flip mechanism for field strengths larger than 1 T at these temperatures. Least-squares fits of Eq. (11) to the experimental rates are plotted in Fig. 4(b), showing excellent agreement with the model. Very similar results were observed independent of Er^{3+} ion concentration, as expected. The experimental value[32] of $g_{env}=6.1$ corresponding to Er^{3+} ions residing at site 1 was used in Eq. (11), leaving R_0 and α_D as the only fit parameters. Values of R_0 and α_D for each sample are summarized in Table I. Assignment of the direct phonon process as the leading spin-lattice relaxation mechanism agrees with temperature-dependent EPR measurements on $Er^{3+}:Y_2SiO_5$ at low fields, which also indicated that the direct process

should remain dominant for temperatures up to several Kelvin.[56]

The field-independent contribution to the spectral diffusion rate, described by R_0, sets the lower limit for the spin-flip rate and becomes more important than the direct process for fields of <1 T. The fact that this component is independent of the field might suggest that it is due to the two-phonon Raman and Orbach processes; however, EPR measurements indicate that the Raman and Orbach rates are much too small at 1.6 K to account for the observed values of R_0.[56] An additional weak, field-independent "anomalous" relaxation process with a linear temperature dependence has been observed in several rare-earth-doped materials at low temperatures[57] and has been attributed to cross-relaxation with paramagnetic impurities in the crystal.[58] That impurity mechanism is likely the leading contribution to the R_0 values that we observed so that crystal purity may place a lower limit on the spectral diffusion rate. In addition, R_0 limits the maximum spectral hole lifetime for the Zeeman sublevel population storage mechanism.

Contributions to spectral diffusion from $Er^{3+}-Er^{3+}$ spin flip-flops would be identified by an increase in the rate at low fields. For the range of magnetic-field strengths and concentrations studied, there was no evidence for increased flip rates, suggesting that the Er^{3+} site-1 flip-flop rates are below the kilohertz level for the conditions investigated here.

C. Homogeneous linewidth

The linewidth given by Γ_0 represents the $t_{12}, T_W \rightarrow 0$ limit of the effective linewidth and describes all dynamic broadening mechanisms that occur faster than the minimum experimental time scales. These effects include the traditional homogeneous linewidth Γ_h that results from lifetime broadening and phase interruptions (the fundamental linewidth of a single ion in the lattice), spectral diffusion processes that occur on very fast time scales, and instantaneous spectral diffusion (ISD).[50,59] The broadening mechanism responsible for ISD is similar to spectral diffusion, except that the random frequency shifts are caused by excitation-induced changes in the ions' environment. As ions in the lattice are excited by the incident light, changes in the excited ions' properties perturb the resonance frequencies of nearby ions, producing an instantaneous spectral diffusion effect. In some cases, the broadening due to this effect can be calculated using an approach similar to the methods described in Sec. IV A.[50,60]

Values of Γ_0 were determined by fitting Eq. (3) to the observed stimulated echo decays, with Γ_{eff} given by Eq. (4). No pronounced variation in Γ_0 with magnetic field was observed except for a slight increase for the lowest fields, perhaps indicating the effects of spin flip-flop processes. Values of Γ_0 averaged over all measured magnetic fields are presented in Table I for each Er^{3+} concentration studied. In contrast to Γ_0, values of T_M determined from two-pulse echo decays[31] showed distinct structure for magnetic fields ranging from 0.3 to 3.0 T that was well described by Eq. (7) using material parameters determined from our more extensive stimulated echo measurements.

The Er^{3+} spin-flip processes also contribute to the homogeneous linewidth through T_1 broadening of the optical transition. Because Er^{3+} spin flips can excite population from the ground state to the upper Zeeman component of the Kramers doublet, the ground-state lifetime T_g contributes an amount $\Delta\Gamma_h = 1/(2\pi T_g)$ to the linewidth. The spectral diffusion rate, which represents the sum of the upward and downward spin-flip transition rates, may be used to estimate the spin-flip contribution to Γ_h. Using Boltzmann statistics to calculate the ratio of the upward and downward spin-flip rates for thermal equilibrium, the broadening of the optical transition due to ground-state spin flips is

$$\Delta\Gamma_h = \frac{R}{4\pi} e^{\frac{-g_g \mu_B B}{2kT}} \operatorname{sech}\left(\frac{g_g \mu_B B}{2kT}\right), \tag{12}$$

where g_g is the ground state g factor. For the rates presented in Fig. 4(b), the ground-state lifetime contributes ~ 50 Hz at the lowest fields and 10 Hz at 2 T. Since the excited-state lifetime is $T_1 = 11.4$ ms for site 1, it contributes only 14 Hz to the linewidth.[32] This shows that the spin-state lifetime can be as important as the excited-state lifetime. Although these contributions are negligible compared to the observed linewidths at low temperatures, this mechanism is an important contribution to the homogeneous linewidth at higher temperatures where the rates are much faster, as will be discussed in Sec. V A.

V. DEPENDENCE OF SPECTRAL DIFFUSION ON CRYSTAL TEMPERATURE

The dependence of spectral diffusion on temperature was investigated in 0.02% $Er^{3+}:Y_2SiO_5$ at a fixed magnetic-field strength of $B = 2.25$ T for temperatures between 1.4 and 2.4 K. The evolution of the effective linewidth in 0.02 % $Er^{3+}:Y_2SiO_5$ is shown in Fig. 3. Solid lines are fits to Eq. (6), giving excellent agreement with the data. The corresponding values of Γ_{SD} and R for each temperature are plotted in Fig. 5. Raising the temperature clearly counteracts the magnetic field's effect on the spectral diffusion, causing the spectral diffusion to increase. From Eq. (9), we see that the magnitude of the spectral diffusion depends on the ratio B/T; consequently, increasing (decreasing) the temperature has an effect on the maximum linewidth equivalent to decreasing (increasing) the magnetic-field strength.

The linewidth broadening and spectral diffusion dynamics were also measured in 0.005% $Er^{3+}:Y_2SiO_5$ at 4.2 K for magnetic fields from 2 to 5 T and for a fixed magnetic field of 6 T for temperatures from 4.2 to 6.5 K. The observed linewidths are plotted in Figs. 6(a) and Fig. 7 as a function of T_W, demonstrating that the spectral diffusion increases and exhibits a complex behavior at higher temperatures.

A. Spectral diffusion due to Er^{3+}

The spectral diffusion linewidths extracted from the temperature-dependent data in Fig. 3 are presented in Fig. 5(a). The very strong temperature dependence of Γ_{SD} is clearly observed as the linewidth increases by more than an order of magnitude for a temperature increase of only 1 K.

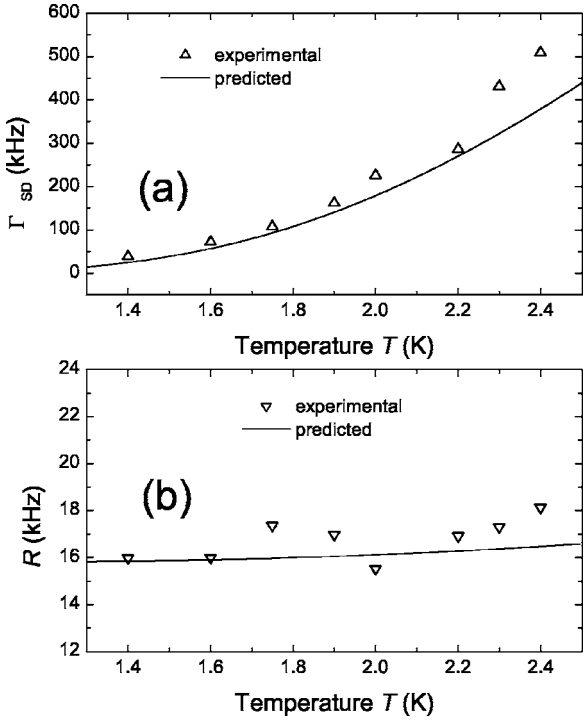

FIG. 5. (a) Measured spectral diffusion linewidth Γ_{SD} and (b) relaxation rate R as a function of temperature for 0.02% $Er^{3+}:Y_2SiO_5$ at $B=2.25$ T. Solid lines show the predicted temperature dependence based on the parameters extracted from the measured magnetic-field dependence.

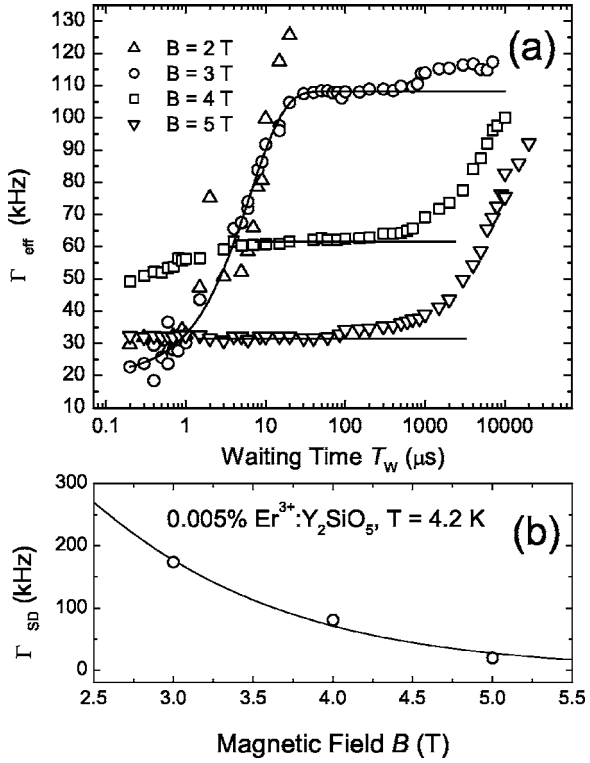

FIG. 6. (a) Evolution of the effective linewidth for site 1 in 0.005% $Er^{3+}:Y_2SiO_5$ at $T=4.2$ K as the waiting time T_W was varied. The magnetic field was varied over the range from $B=2$ T to $B=5$ T between data sets. The solid line at $B=3$ T is a least-squares fit to the data using Eq. (6); solid lines at 4 and 5 T denote the maximum level of the Er^{3+} contribution to the spectral diffusion. (b) Measured Er^{3+} contribution to the spectral diffusion linewidth Γ_{SD} as a function of magnetic field for 0.005% $Er^{3+}:Y_2SiO_5$ at 4.2 K. The solid line is a least-squares fit using Eq. (9).

The solid line in Fig. 5(a) represents the temperature dependence predicted by Eq. (9) with the value of Γ_{max} determined from the magnetic-field dependence of the linewidth (see Table I). The agreement between data and calculation is very good since an uncertainty in the temperature of only ±0.1 K causes the linewidth to change by up to 40%. This also demonstrates that understanding the magnetic-field dependence provides insight into the temperature dependence. The temperature dependence of R, predicted from the magnetic-field dependence using Eq. (11) and the parameters given in Table I, is plotted in Fig. 5(b), showing good agreement with the observed values.

The behavior of the linewidth at 4.2 K depicted in Fig. 6(a) exhibits spectral diffusion components with two distinct time scales. This is most apparent in the data at 4 T, where one spectral diffusion mechanism reaches its maximum effect at the earliest time scales of ~1 μs, while the second mechanism is just beginning to act at the longest time scales of ~1 ms. We expect one of these spectral diffusion components to result from Er^{3+} ions residing at site 1, while Er^{3+} ions residing at site 2 and ^{89}Y nuclear spins are potential candidates for the other component. The strong magnetic-field dependence of the faster component, where the broadening decreases from >130 kHz at 2 T to only ~10 kHz at 5 T in Fig. 6(a), suggests that it is due to Er^{3+} ions. Using Eqs. (8) and (9) to estimate the relative spectral diffusion broadening at 4.2 K from sites 1 and 2, we found that the site-1 contribution matches the observed magnitude of the fast spectral diffusion component as shown in Fig. 6(b). We also found that, for $\boldsymbol{B}\|\boldsymbol{D}_1$, the site-2 contribution should be at least an order of magnitude smaller than the site-1 contribution for all of the temperatures and magnetic-field strengths that we examined; consequently, the remaining slow compo-

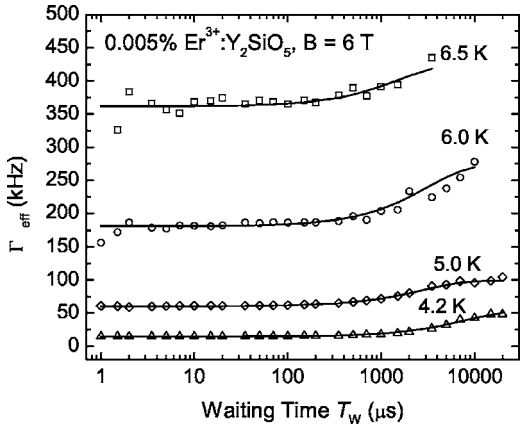

FIG. 7. Evolution of the effective linewidth for site 1 in 0.005% $Er^{3+}:Y_2SiO_5$ at $B=6$ T as the waiting time T_W was varied. The temperature was varied over the range from $T=4.2$ K to $T=6.5$ K. Solid lines are least-squares fits to the data using Eq. (6).

nent was attributed to ^{89}Y nuclear spin flips discussed in Sec V B.

In Fig. 6(a), only the data at 3 T clearly show the full evolution of the site 1 Er^{3+} spectral diffusion component, making a thorough analysis of the spectral diffusion parameters difficult; however, we can extract useful information about the dynamics. Fitting Eq. (6) to the evolution of the linewidth at 3 T, we obtain the parameters $\Gamma_0 = 22$ kHz, $\Gamma_{SD} = 174$ kHz, and $R = 153$ kHz. Furthermore, the saturation level of the Er^{3+} spectral diffusion component was clearly observed for all fields above 2 T, as indicated in Fig. 6(a) by the solid horizontal lines. If we assume that Γ_0 is approximately constant for different fields, as was observed at 1.6 K, we may use the value extracted from the 3 T data to determine the Γ_{SD} contribution to the linewidth broadening at 4 T and 5 T. The estimated values of Γ_{SD} for each field are plotted in Fig. 6(b), and the solid line is the fit of Eq. (9). The corresponding value of Γ_{max} is presented in Table I, giving reasonable agreement with the value determined from the 1.6 K data.

Less information may be extracted regarding the spectral diffusion rate at 4.2 K since R can only be reliably determined for the data set at 3 T. If we use the average value of $\alpha_D \sim 1.13 \times 10^{-3}$ kHz/T^5 for the direct phonon process, as indicated by the data at 1.6 K (see Table I), we predict values of $R \sim 10$ kHz at 2 T, $R \sim 70$ kHz at 3 T, $R \sim 270$ kHz at 4 T, and $R \sim 810$ kHz at 5 T. Although these results agree qualitatively with the observed behavior, the measured rates appear to be larger than the values predicted from the direct phonon process alone, suggesting that other Er^{3+} spin-flip mechanisms contribute significantly to the rate at 4.2 K.

Figure 7 shows the effective linewidth Γ_{eff} at a fixed magnetic field of $B = 6$ T as the temperature was increased from $T = 4.2$ K to $T = 6.5$ K. To our knowledge, $T = 6.5$ K corresponds to the highest temperature at which photon echoes have ever been observed in any Er^{3+}-activated material. As the temperature was raised, a substantial increase in Γ_{eff} from 15 kHz at 4.2 K to 360 kHz at 6.5 K was observed over all time scales. Because the expected Er^{3+} spectral diffusion contribution to Γ_{eff} is only 5 kHz at 4.2 K and 40 kHz at 6.5 K for this field, the large increase observed in Γ_{eff} was attributed to an increase in Γ_0 caused by the temperature-dependent broadening of the homogeneous linewidth. In fact, the temperature dependence is well described by Eq. (12) with R given by Eq. (10), although the individual contributions from each spin-flip process cannot be distinguished without additional data over a wider temperature range. In addition to lifetime broadening, other decoherence mechanisms, such as elastic phonon scattering, also become important at these higher temperatures and contribute to the increase in Γ_0.

A second spectral diffusion component also appears in Fig. 7 for time scales longer than 1 ms. This effect was similar to the behavior observed in Fig. 6(a) and was attributed to ^{89}Y nuclear spin flips, as discussed in Sec. V B.

B. Spectral diffusion due to ^{89}Y nuclear spins

Because the ^{89}Y nuclear spins have very slow flip rates and have a significant magnetic dipole-dipole interaction with neighboring Er^{3+} ions, we expect that the spectral diffusion component observed at the longest time scales in the data at 4.2 K and above is due to ^{89}Y spins in the host lattice. Although the full behavior of the ^{89}Y contribution was not observed over the time scales of the Er^{3+} spectral hole lifetime, we may draw important conclusions about the nuclear spin dynamics by comparing the data to theoretical models. In describing the behavior of the spectral diffusion, it is important to recognize that there are several essential differences between the broadening due to $Er^{3+}-Er^{3+}$ interactions and $Er^{3+}-{}^{89}$Y interactions. For example, the time evolution of the effective linewidth can be different from Eq. (4) since broadening due to a concentrated spin system is often considered to be a Gaussian diffusion process,[1–4,45] with approximately Gaussian line shapes expected for spin concentrations greater than $\sim 10\%$.[43] This would cause the t_{12} and T_W terms in the effective linewidth to be replaced by the square roots of the terms in Eq. (4).[3,5] Even so, both numerical calculations of the spectral diffusion due to nuclear spins[61] and the fact that exponential decays are observed at large values of T_W indicate that the spectral diffusion can be described by a Lorentzian diffusion process for this material. This may suggest that only a small number of ^{89}Y spins in the environment contribute to the observed Er^{3+} spectral diffusion, perhaps because of the effects discussed later in this section.

To describe the spectral diffusion caused by $Er^{3+}-{}^{89}$Y interactions, we must include another term in Eq. (4) with the two additional parameters Γ_{YSD} and R_Y to characterize the ^{89}Y-induced broadening. Although each Er^{3+} impurity experiences a random environment of Er^{3+} perturbers, every Er^{3+} experiences the same arrangement of ^{89}Y spins determined by the crystal structure; consequently, the methods used to describe the magnitude of spectral diffusion caused by Er^{3+} impurities may not be directly applied to Γ_{YSD}. Following the "method-of-moments" approach commonly used for calculating the dipolar linewidth due to an environment of concentrated spins, we may estimate the total ^{89}Y contribution to the Er^{3+} spectral diffusion as

$$\Gamma_{YSD} = 0.14\mu_0\gamma_Y|g_g - g_e|\mu_B n_Y\sqrt{I(I+1)}\,\mathrm{sech}\left(\frac{h\gamma_Y B}{2kT}\right), \tag{13}$$

where $\gamma_Y = 2.1$ MHz/T is the ^{89}Y gyromagnetic ratio in frequency units (defined by $\nu = \gamma B$), the nuclear spin of ^{89}Y is $I = 1/2$, n_Y is the total density of ^{89}Y in the lattice (including both sites), and all other quantities are the same as before. Because of the low C_1 symmetry of the Y sites, we have used the Van Vleck equation[40,42] for the dipolar broadening in a powder of cubic crystallites. Furthermore, we have explicitly included the temperature dependence of the dipolar linewidth[41,51,52] and assumed a Gaussian line shape, as commonly used when describing concentrated spin systems.[1,40,42] To test the accuracy of these approximations, the same approach used to obtain Eq. (13) was used to calculate the ^{89}Y nuclear resonance linewidth, including the additional nuclear flip-flop contribution, giving a value of 21 Hz. This is in reasonable agreement with the experimentally measured ^{89}Y

linewidth of 35 Hz for Y_2SiO_5,[62] providing an indication of the accuracy obtained using the simple approximations for the crystal structure and dipolar line shape.

From Eq. (13), the predicted contribution to the spectral diffusion broadening Γ_{YSD} due to ^{89}Y nuclear spins is 60 kHz. Because the ^{89}Y nuclear magnetic moment is very small, the broadening is essentially independent of the temperature and magnetic-field strength for any experimentally achievable values, providing a clear signature of nuclear contributions to spectral diffusion. For the 5 T data shown in Fig. 6(a), the estimated broadening due to ^{89}Y reaches a level of 60 kHz at the longest time scales, corresponding to a Γ_{YSD} of ~120 kHz [see Eq. (6)]. From the temperature dependent data in Fig. 7, the ^{89}Y contribution to the linewidth indicates similar values of Γ_{SD} between 70 and 100 kHz. These values agree reasonably well with the calculated value, considering the uncertainties in the calculation and measurements, particularly since limited laser frequency stability and reduced signal-to-noise make it difficult to measure photon echoes for the very long time scales required to observe the ^{89}Y spectral diffusion.

We see that the ^{89}Y spectral diffusion rates noticeably increase with magnetic field so that they are too slow to observe at low fields and are on the order of ~100 Hz at the highest fields. To understand this behavior, we must consider the nuclear spin-flip mechanisms. For ^{89}Y in a pure Y_2SiO_5 host crystal, we expect the nuclear spin-lattice relaxation rates to be very slow so that the dominant spin-flip mechanism would be nuclear flip-flops; however, the large Er^{3+} magnetic moments strongly perturb neighboring ^{89}Y spins so that their properties deviate significantly from the properties of unperturbed spins in the bulk of the crystal.

One effect of the Er^{3+} ion's magnetic field is to shift the frequencies of nearby spins as a function of distance from the Er^{3+} ion so that neighboring spins are no longer resonant with each other, inhibiting the nuclear spin flip-flop process. This causes the well-known "frozen-core" effect in which the flip-flop rates of spins near a paramagnetic impurity are dramatically reduced from the bulk flip-flop rate.[4,63–65] As a result, we must separately consider the spectral diffusion due to normal bulk nuclear spins, and the spectral diffusion due to nuclear spins within the frozen core that surrounds the paramagnetic ion so that $\Gamma_{YSD}=\Gamma_{bulk}+\Gamma_{core}$. A rough estimate for the relative magnitude of these two components has been obtained by Mims,[4] giving

$$\Gamma_{bulk} \sim 0.73\Gamma_{YSD}\sqrt{\frac{\gamma_Y}{\gamma_{Er}}}. \tag{14}$$

Because the Er^{3+} gyromagnetic ratio is $\sim 10^4$ times larger than the ^{89}Y nuclear gyromagnetic ratio, Eq. (14) predicts that the unperturbed bulk ^{89}Y spins only contribute less than 1% to the total spectral diffusion linewidth; consequently, the Er^{3+} spectral diffusion due to ^{89}Y is almost entirely determined by the dynamics of the frozen core (i.e., $\Gamma_{YSD} \sim \Gamma_{core}$).

The distribution of flip-flop rates within the frozen core may be estimated by considering the magnitude of the Er^{3+} field at each ^{89}Y and using Fermi's Golden Rule to calculate the effect on the flip-flop probabilities.[4,65] However, it is instructive to first consider the bulk ^{89}Y flip-flop rate, which places an upper limit on the rate within the frozen core. The bulk flip-flop rates[40,55] are related to the second moment of the $^{89}Y-^{89}Y$ dipolar interaction,[42,51,52] and may be estimated as

$$R_{Yff} \sim 0.25\mu_0 h\gamma_Y^2 n_Y \sqrt{I(I+1)}\,\mathrm{sech}\left(\frac{h\gamma_Y B}{2kT}\right). \tag{15}$$

For Y_2SiO_5, ^{89}Y nuclei at sites 1 and 2 have significantly different chemical shifts of their gyromagnetic ratios and are not resonant with each other;[62] as a result, mutual flip-flops cannot occur between ^{89}Y at different crystallographic sites so that n_Y in Eq. (15) corresponds to the ^{89}Y concentration for each individual site. Using Eq. (15), we find that the ^{89}Y flip-flop rate for Y_2SiO_5 is ~8 Hz for all magnetic fields studied here. Because the flip-flop rates within the frozen core are expected to be much slower than the bulk rate, nuclear flip-flops cannot account for the observed behavior.

To explain the observed ^{89}Y flip rates, we must consider the effect of Er^{3+} ions on the ^{89}Y nuclear spin-lattice relaxation. Although the spin-lattice relaxation rate of bulk ^{89}Y spins is typically much less than 1 Hz,[66] the dipole-dipole interaction with Er^{3+} can cause the relaxation rate of ^{89}Y near the Er^{3+} to be much faster.[8,40,65,66] It is important to point out that this effect is not due to mutual flip-flops, but occurs through $S_zI_\pm$ terms in the dipolar Hamiltonian (where S_z is the z component of the electron effective spin operator and $I_\pm$ is the raising/lowering operator for the nuclear spin) and therefore does not affect the state of the Er^{3+} ion.[40] The magnitude of this effect is given by Abragam[40] for the limit $R \ll 2\pi\gamma_Y B$, so that the contribution to the spin-lattice relaxation rate R_Y of each ^{89}Y nuclear spin is approximately

$$R_Y = \frac{3\mu_0^2 g_g^2 \mu_B^2}{160\pi^2 B^2 r^6} R, \tag{16}$$

where r is the distance of the ^{89}Y nucleus from Er^{3+} and all other quantities have the same meaning as before. Since the Er^{3+} flip rates are determined by the direct phonon process, which is approximately proportional to B^5 and independent of temperature in the high-field limit, Eq. (16) predicts that the ^{89}Y flip rate will increase as B^3, qualitatively agreeing with the observed increase in the rate for higher fields. Because this contribution to the ^{89}Y relaxation rate decreases as the sixth power of the $Er^{3+}-^{89}Y$ distance, it will only have a significant effect on the nearest neighbors of the Er^{3+} ion. However, we may use the same approach as used to obtain Eq. (14) to show that the nearest neighbors account for ~50% of the total ^{89}Y contribution to the broadening. In fact, numerical calculations of the spectral diffusion due to nuclear spins indicate that the nearest neighbors are even more important than predicted by this simple estimate.[64,67] This is likely the reason why broadening due to ^{89}Y can be successfully described using the Lorentzian spectral diffusion model.

If we use the estimated Er^{3+} rates at 4.2 K in Eq. (16), we obtain ^{89}Y nearest-neighbor flip rates of 26 Hz at 3 T and 110 Hz at 5 T, consistent with the observed behavior. Furthermore, the estimated Er^{3+}-induced ^{89}Y nuclear flip rates

are <20 Hz for all the data taken at 1.6 K, which explains why this effect was not observed in the 1.6 K data over the measured time scales.

For the temperature-dependent data in Fig. 7, the ^{89}Y spectral diffusion rate appears to increase from ~ 100 Hz at 4.2 K to ~ 1 kHz at 6.5 K, although the large homogeneous linewidths at higher temperatures make it difficult to analyze the ^{89}Y broadening quantitatively. Although Eqs. (16) and (11) indicate a weak temperature dependence for the ^{89}Y spectral diffusion rate when the Er^{3+} rate is dominated by the direct process, the other processes in Eq. (10) become more important at higher temperatures and cause a much stronger temperature dependence.

VI. DEPENDENCE OF SPECTRAL DIFFUSION ON Er^{3+} CONCENTRATION

To explore the effect of Er^{3+} concentration on spectral diffusion, the evolution of the effective linewidth was examined under a variety of conditions. The magnetic-field dependence for concentrations of 0.02%, 0.005%, and 0.0015% at 1.6 K is presented in Fig. 2. By comparing the observed linewidths, we clearly observe that the spectral diffusion is significantly reduced for lower Er^{3+} concentrations, highlighting the role of $Er^{3+}-Er^{3+}$ interactions as the source of broadening.

From Eq. (8), we see that the spectral diffusion is directly proportional to the Er^{3+} concentration in the crystal. Thus, the concentration dependence may be described by an equation of the form

$$\Gamma_{\max} = \alpha_c c, \tag{17}$$

where c is the Er^{3+} concentration and α_c is a constant. Fitting Eq. (17) to the three experimental values of $\Gamma_{\max}$ for $T=1.6$ K listed in Table I gives $\alpha_c = 230$ MHz/%.

The value of Γ_0 shows a weak dependence on concentration, increasing by a factor of four as the concentration was increased from 0.0015 to 0.02 %. This effect was attributed to a slight increase in the instantaneous spectral diffusion that arises from the larger absorption of the higher concentration samples; however, to confirm this explanation, further intensity-dependent measurements of the linewidth are required.

The spectral diffusion rate parameters R_0 and α_D given in Table I were independent of Er^{3+} concentration. As the concentration was increased from 0.0015 to 0.02 %, the value of α_D remained constant, while R_0 stayed below 1 kHz. This behavior was anticipated since the Er^{3+} concentration should not affect the magnitude of the direct phonon coupling coefficient. Finally, we note that $Er^{3+}-Er^{3+}$ spin flip-flop processes are expected to become more important as the concentration is increased so that, although they are not observed in our data, they may make important contributions to the rate for concentrations higher than those studied here.

VII. SUMMARY AND CONCLUSIONS

With the dual goals of characterizing the $Er^{3+}:Y_2SiO_5$ material and expanding the understanding of spectral diffusion in paramagnetic materials more generally, the dynamic optical properties of the paramagnetic material $Er^{3+}:Y_2SiO_5$ were studied in detail. Photon echo spectroscopy and extensive modeling of the spin dynamics were used to characterize the increase in decoherence over time scales from 1 μs to 20 ms for magnetic-field strengths from 0.3 to 6.0 T, temperatures from 1.6 to 6.5 K, and Er^{3+} concentrations of 0.0015%, 0.005%, and 0.02%. Measurements at 6.5 K reported here are, to our knowledge, the highest temperature photon echoes observed in any Er^{3+}-activated material; the observation of coherent processes at these more accessible temperatures greatly improves the prospects for applications of Er^{3+} materials in SHB and SSH devices and in quantum computing or quantum information systems.

The influence of spectral diffusion on the observed stimulated echo decay curves was described by detailed models for the magnitude and rate of the dynamic perturbations affecting the ion transition frequencies. Using this approach, the observed evolution of the effective linewidth could be accurately described and predicted. The temperature and magnetic-field dependence of the maximum spectral diffusion linewidth identified spin flips of Er^{3+} ions at crystallographic site 1 as the predominant source of spectral diffusion for a magnetic field applied along $\boldsymbol{D}_1$ at low temperatures. The temperature and magnetic field dependence of the spectral diffusion rate distinguished the direct phonon process as the dominant Er^{3+} spin flip mechanism. In addition to spectral diffusion caused by spin flips of the site 1 Er^{3+} ions, spectral diffusion due to ^{89}Y nuclear spin flips was evident at 4.2 K and above for time scales exceeding ~ 1 ms.

Using the extensive collection of data presented here, spectral diffusion was comprehensively modeled and quantitatively described over a wide range of operating conditions and material parameters. The simple models were extremely successful in describing, explaining, and predicting spectral diffusion and its effects on optical decoherence, providing a valuable alternative to more elaborate numerical simulations. We have also demonstrated how fundamental understanding of the basic material physics provides essential insights into the complicated behavior caused by spectral diffusion. This insight, coupled with detailed model projections, can now guide material design and identify operating points that enhance the capabilities of SSH and SHB optical technologies by allowing optimum conditions to be predicted from a few selected measurements not only for Er^{3+} materials, but also for other paramagnetic materials such as those containing Nd^{3+} or Yb^{3+}. The work presented here has enabled optical processing in $Er^{3+}:Y_2SiO_5$ to be extended to higher bandwidth[16] at higher cryocooler temperatures and also has enabled the measurement of what we believe to be the narrowest optical resonance in a solid with a homogeneous linewidth of 73 Hz.[23] Additional high bandwidth demonstrations are in progress.

ACKNOWLEDGMENTS

The authors are grateful to R. W. Equall and R. L. Hutcheson of Scientific Materials Corporation of Bozeman,

MT, for providing the crystals and to R. M. Macfarlane for many valuable discussions. All experimental measurements were conducted at Montana State University. This research was supported by the U.S. Air Force Office of Scientific Research Grant No. F49620-01-1-0313 and Montana Board of Research and Commercialization Technology.

*Permanent address: Department of Physics, University of San Francisco. Electronic address: tbottger@usfca.edu
†Electronic address: thiel@physics.montana.edu
‡Present address: Department of Physics, University of South Dakota, Vermillion, SD 57069, USA. Electronic address: ycsun@usd.edu
§Electronic address: cone@montana.edu

[1] B. Herzog and E. L. Hahn, Phys. Rev. **103**, 148 (1956).
[2] J. R. Klauder and P. W. Anderson, Phys. Rev. **125**, 912 (1962).
[3] W. B. Mims, Phys. Rev. **168**, 370 (1968).
[4] W. B. Mims, in *Electron Paramagnetic Resonance*, edited by S. Geschwind (Plenum, New York, 1972), p. 263.
[5] P. Hu and S. R. Hartmann, Phys. Rev. B **9**, 1 (1974).
[6] P. Hu and L. R. Walker, Phys. Rev. B **18**, 1300 (1978).
[7] R. M. Macfarlane and R. M. Shelby, Opt. Commun. **42**, 346 (1982).
[8] R. Wannemacher, R. S. Meltzer, and R. M. Macfarlane, J. Lumin. **45**, 307 (1990).
[9] J. Ganem, Y. P. Wang, D. Boye, R. S. Meltzer, W. M. Yen, and R. M. Macfarlane, Phys. Rev. Lett. **66**, 695 (1991).
[10] R. Yano, M. Mitsunaga, and N. Uesugi, Phys. Rev. B **45**, 12752 (1992).
[11] Y. C. Sun, in *Spectroscopic Properties of Rare Earths in Optical Materials*, edited by Guokui Liu and B. Jacquier (Springer, Berlin and Tsingua University Press, 2005), p. 379.
[12] H. Lin, T. Wang, and T. W. Mossberg, Opt. Lett. **20**, 1658 (1995).
[13] T. L. Harris, Y. Sun, R. L. Cone, R. M. Macfarlane, and R. W. Equall, Opt. Lett. **23**, 636 (1998).
[14] T. L. Harris, Y. Sun, W. R. Babbitt, J. A. Ritcey, and R. W. Equall, Opt. Lett. **25**, 85 (2000).
[15] A. Renn, U. P. Wild, and A. Rebane, J. Phys. Chem. A **106**, 3045 (2002).
[16] Z. Cole, T. Böttger, R. Krishna Mohan, R. Reibel, W. R. Babbitt, R. L. Cone, and K. D. Merkel, Appl. Phys. Lett. **81**, 3525 (2002).
[17] V. Crozatier, V. Lavielle, F. Bretenaker, J.-L. Le Gouët, and I. Lorgeré, IEEE J. Quantum Electron. **40**, 1450 (2004).
[18] F. Schlottau and K. Wagner, J. Lumin. **107**, 90 (2004).
[19] K. D. Merkel, R. K. Mohan, Z. Cole, T. Chang, A. Olson, and W. R. Babbitt, J. Lumin. **107**, 62 (2004).
[20] P. B. Sellin, N. M. Strickland, T. Böttger, J. L. Carlsten, and R. L. Cone, Phys. Rev. B **63**, 155111 (2001).
[21] G. J. Pryde, T. Böttger, and R. L. Cone, J. Lumin. **98**, 309 (2002).
[22] Thomas Böttger, G. J. Pryde, and R. L. Cone, Opt. Lett. **28**, 200 (2003).
[23] Thomas Böttger, Y. Sun, C. W. Thiel, and R. L. Cone, Proc. SPIE **4988**, 51 (2003).
[24] M. D. Lukin and P. R. Hemmer, Phys. Rev. Lett. **84**, 2818 (2000).
[25] N. Ohlsson, R. K. Mohan, and S. Kröll, Opt. Commun. **201**, 71 (2002).
[26] J. J. Longdell, M. J. Sellars, and N. B. Manson, Phys. Rev. Lett. **93**, 130503 (2004).
[27] Y. Zhang, X. A. Shen, and R. Kachru, Opt. Lett. **22**, 1068 (1997).
[28] Thomas Böttger, Y. Sun, G. J. Pryde, G. Reinemer, and R. L. Cone, J. Lumin. **94-95**, 565 (2001).
[29] M. Mitsunaga, R. Yano, and N. Uesugi, Opt. Lett. **16**, 23 (1991).
[30] R. W. Equall, Y. Sun, R. L. Cone, and R. M. Macfarlane, Phys. Rev. Lett. **72**, 2179 (1994).
[31] R. M. Macfarlane, T. L. Harris, Y. Sun, R. L. Cone, and R. W. Equall, Opt. Lett. **22**, 871 (1997).
[32] Thomas Böttger, Ph.D. thesis, Montana State University, 2002.
[33] V. Crozatier, G. Gorju, F. Bretenaker, J.-L. Gouët, and I. Lorgeré, Opt. Lett. **30**, 1288 (2005).
[34] Thomas Böttger, C. W. Thiel, Y. Sun, and R. L. Cone (unpublished).
[35] B. A. Maksimov, Yu. A. Kharitonov, V. V. Ilyukhin, and N. B. Belov, Sov. Phys. Dokl. **13**, 1188 (1969).
[36] Y. Sun, F. Könz, R. L. Cone, and R. W. Equall (unpublished).
[37] C. Li, C. Wyon, and Richard Moncorgé, IEEE J. Quantum Electron. **28**, 1209 (1992).
[38] R. M. Macfarlane and R. M. Shelby, in *Spectroscopy of Solids Containing Rare Earth Ions*, edited by A. A. Kaplyanskii and R. M. Macfarlane (North Holland, Amsterdam, 1987), p. 51.
[39] M. D. Levenson and S. S. Kano, *Introduction to Nonlinear Laser Spectroscopy* (Academic Press, New York, 1988), p. 228, and references cited therein.
[40] A. Abragam, *The Principles of Nuclear Magnetism* (Oxford University Press, London, 1961).
[41] A. Abragam and B. Bleaney, *Electron Paramagnetic Resonance of Transition Ions* (Oxford University Press, London, 1970).
[42] J. H. Van Vleck, Phys. Rev. **74**, 1168 (1948).
[43] C. Kittel and E. Abrahams, Phys. Rev. **90**, 238 (1953).
[44] Y. S. Bai and M. D. Fayer, Phys. Rev. B **39**, 11066 (1989).
[45] W. B. Mims, K. Nassau, and J. D. McGee, Phys. Rev. **123**, 2059 (1961).
[46] N. Bloembergen, E. M. Purcell, and R. V. Pound, Phys. Rev. **73**, 679 (1948).
[47] Y. Sun, R. M. Macfarlane, and R. L. Cone (unpublished).
[48] R. M. Macfarlane and J. C. Vial, Phys. Rev. B **36**, 3511 (1987).
[49] G. K. Liu, Jin Huang, R. L. Cone, and B. Jacquier, Phys. Rev. B **38**, 11061 (1988).
[50] G. K. Liu and R. L. Cone, Phys. Rev. B **41**, 6193 (1990).
[51] M. McMillan and W. Opechowski, Can. J. Phys. **38**, 1168 (1960).
[52] I. Svare and G. Seidel, Phys. Rev. **134**, A172 (1964).
[53] A. G. Maryasov, S. A. Dzuba, and K. M. Salikhov, J. Magn. Reson. (1969-1992) **50**, 432 (1982).
[54] R. Orbach and H. J. Stapleton, in *Electron Paramagnetic Resonance*, edited by S. Geschwind (Plenum, New York, 1972), p. 121.
[55] A. M. Portis, Phys. Rev. **104**, 584 (1956).
[56] I. N. Kurkin and K. P. Chernov, Physica B & C **101**, 233 (1980).
[57] E. S. Sabisky and C. H. Anderson, Phys. Rev. B **1**, 2028 (1970).
[58] M. M. Broer and W. M. Yen, Phys. Rev. B **23**, 3686 (1981).
[59] J. Huang, J. M. Zhang, A. Lezama, and T. W. Mossberg, Phys.

Rev. Lett. **63**, 78 (1989).
[60] F. R. Graf, A. Renn, G. Zumofen, and U. P. Wild, Phys. Rev. B **58**, 5462 (1998).
[61] J. P. Hurrell and E. R. Davies, Solid State Commun. **9**, 461 (1971).
[62] R. Dupree and M. E. Smith, Chem. Phys. Lett. **148**, 41 (1988).
[63] R. M. Shelby, C. S. Yannoni, and R. M. Macfarlane, Phys. Rev. Lett. **41**, 1739 (1978).
[64] R. G. DeVoe, A. Wokaun, S. C. Rand, and R. G. Brewer, Phys. Rev. B **23**, 3125 (1981).
[65] Y. P. Wang, D. P. Landau, R. S. Meltzer, and R. M. Macfarlane, J. Opt. Soc. Am. B **9**, 946 (1992).
[66] R. H. Meinhold and K. J. D. MacKenzie, Solid State Nucl. Magn. Reson. **5**, 151 (1995).
[67] Y. S. Bai and R. Kachru, Phys. Rev. A **44**, R6990 (1991).